CHALMERS
UNIVERSITY OF TECHNOLOGY

Phase-Only Positioning: Overcoming Integer Ambiguity Challenge Through Deep Learning

Citation for the original published paper (version of record):

Ayten, F., Ilter, M., Kaltiokallio, O. et al (2025). Phase-Only Positioning: Overcoming Integer Ambiguity Challenge Through Deep Learning. IEEE International Symposium on Personal, Indoor and Mobile Radio Communications, PIMRC.
http://dx.doi.org/10.1109/PIMRC62392.2025.11275391

Phase-Only Positioning: Overcoming Integer Ambiguity Challenge through Deep Learning

Fatih Ayten*, Mehmet C. Ilter*, Ossi Kaltiokallio*, Jukka Talvitie*, Akshay Jain†,
Elena Simona Lohan*, Henk Wymeersch‡, and Mikko Valkama*
* Electrical Engineering Unit, Tampere Wireless Research Center, Tampere University, Finland
† Radio Systems Research, Nokia Bell Labs, Espoo, Finland
‡Department of Electrical Engineering, Chalmers University of Technology, Sweden
Email: fatih.ayten@tuni.fi, mehmet.ilter@tuni.fi, ossi.kaltiokallio@tuni.fi, jukka.talvitie@tuni.fi,
akshay.2.jain@nokia-bell-labs.com, elena-simona.lohan@tuni.fi, henkw@chalmers.se, mikko.valkama@tuni.fi

***Abstract*—This paper investigates the uplink carrier phase positioning (CPP) in cell-free (CF) or distributed-antenna-system context, assuming a challenging case where only the phase measurements are utilized as observations. In general, CPP can achieve sub-meter to centimeter-level accuracy but it is challenged by the integer ambiguity problem. In this work, we propose two deep learning approaches for phase-only positioning, overcoming the integer ambiguity challenge. The first one directly uses the phase measurements, while the second one first estimates the integer ambiguities and then it integrates them with the phase measurements for improved accuracy. Our numerical results demonstrate that an inference complexity reduction of two to three orders of magnitude is achieved, compared to the maximum likelihood baseline solution, depending on the approach and on the parameter configuration. This emphasizes the potential of the developed deep learning solutions for efficient and precise positioning in future CF 6G systems.**

***Index Terms*—6G, carrier phase positioning, cell-free, deep learning, integer ambiguities, neural networks.**

I. Introduction

Carrier phase positioning (CPP) is an established approach in global navigation satellite systems [1], [2], and it is currently receiving growing interest also in the context of mobile networks towards centimeter-level terrestrial positioning [3]–[6]. CPP is subject to the so-called integer ambiguity challenge, as the mapping of the transmitter-receiver distance to the observable carrier phase is invariant to any integer amounts of wavelengths [1], [7]. Existing solutions include differential phase measurements, hybrid time-phase estimation, and multipath-assisted ambiguity resolution [8]. Additionally, while traditional maximum likelihood estimation (MLE) methods suffer from high computational complexity [9], data-driven techniques, leveraging neural networks (NNs) and clustering-based estimators for ambiguity resolution, have been recently developed [10], [11].

In terrestrial networks, CPP is relevant in the context of distributed multiple-input multiple-output (MIMO) and cell-free (CF) systems – an important and emerging paradigm towards 6G [1], [12], [13]. CF and other distributed MIMO systems eliminate traditional cell boundaries by distributing large numbers of transmission/reception or antenna points (APs) over wide areas. Especially with phase-coherent APs, such a distributed approach offers tempting prospects also for sensing and localization in the effective near-field domain [14], [15].

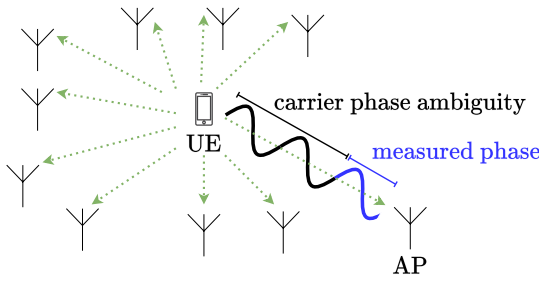

Fig. 1. Conceptual illustration of uplink positioning with distributed antenna points (APs) where only the carrier phase measurements at different APs are used to estimate the UE position.

In general, most existing CPP studies such as [3], [5], [6], [16] combine carrier phase measurements as *additional observations* with more common positioning-related measurements such as time-of-arrival (ToA). The same applies also implicitly to the direct positioning methods described in [14], [15], [17] which harness directly the raw I/Q received signals for localization purposes – embedding the complete channel state information (CSI). To the best of the authors' knowledge, there are no existing terrestrial radio-positioning works that rely exclusively on carrier phase measurements for localizing the user equipment (UE). The only exception is the near-field UE localization using phase-difference type of measurements, however, assuming a large co-located antenna array with classical half-wavelength element spacing, such as [18].

Inspired by the above, this paper seeks to fill this important gap and addresses the *phase-only UE positioning paradigm* and the related integer ambiguity challenge in CF/distributed MIMO system context – illustrated conceptually in Fig. 1. The use of only the carrier phase measurements offers remarkable implementation benefits, as ToA and other related CSI measurements are always subject to hardware impairments, such as the inevitable UE clock bias [1], [16]. To this end, two alternative deep learning based UE positioning approaches are proposed harnessing only the distributed carrier phase

measurements. The first approach, called direct phase-only CPP, utilizes a multi-layer perceptron (MLP) to directly infer position estimates from raw carrier phase measurements. The second approach, entitled integer ambiguity-aided CPP, employs a convolutional neural network (CNN) with a dedicated MLP-based module for integer ambiguity estimation, which is then combined with phase data for improved localization accuracy. To assess their practical feasibility, we analyze the computational complexity of both approaches in terms of floating-point operations (FLOPs) and compare them with the more ordinary MLE-based reference approach. Our results demonstrate that the proposed deep learning approaches not only outperform traditional MLE-based methods in terms of the achievable positioning accuracy for fixed processing complexity in terms of FLOPs, but also obtain really high, centimeter-level, positioning accuracy with largely improved computational efficiency. These findings pave the way for real-time carrier phase-based positioning in future 6G distributed MIMO or cell-free networks.

II. System Model and Baseline

We consider an uplink scenario consisting of a UE and I distributed and mutually phase-synchronized APs. An example scenario with ten APs is shown in Fig. 1. The UE has an unknown position $\boldsymbol{x}_{\text{ue}} \in \mathbb{R}^2$ whereas the APs have known positions $\boldsymbol{x}_{\text{ap},i} \in \mathbb{R}^2$ for $i \in \{0, \dots I-1\}$, with the scenario being extendable to $\mathbb{R}^3$.

When the UE transmits a unit-power narrowband pilot symbol s occupying a bandwidth W with a transmit power P, the received signal at the i-th AP over the line-of-sight (LoS) link reads

$$y_i = \sqrt{E}\rho_i \exp(-j(\frac{2\pi}{\lambda}d_i - \theta))s + v_i, \tag{1}$$

where $E = P/W$ is the symbol energy, ρ_i is the path loss from the UE to the i-th AP, $d_i = \|\boldsymbol{x}_{\text{ue}} - \boldsymbol{x}_{\text{ap},i}\|$ is the Euclidean distance between the UE and the i-th AP, θ is the common phase offset between the UE and the AP network, and $v_i \sim \mathcal{CN}(0, N_0)$ represents additive white complex Gaussian noise. By processing y_i, the resulting phase observations can be formulated as

$$r_i = -\frac{2\pi}{\lambda}d_i + \theta + 2\pi z_i + n_i, \tag{2}$$

where $z_i \in \mathbb{Z}$ is the integer ambiguity, and we model $n_i \sim \mathcal{N}(0, \sigma_i^2)$. From (2), we can take one AP as reference, e.g., $i = 0$, and compute *differential measurements* as

$$\delta_m = -\frac{\lambda}{2\pi}(r_m - r_0) = \Delta_m + k_m\lambda + w_m, m \in \{1, \dots, I-1\}, \tag{3}$$

where $\Delta_m = d_m - d_0$, $k_m = z_0 - z_m$ and $w_m = (\lambda/2\pi)(n_0 - n_m)$. It is also assumed that the maximum delay difference between the reference AP and the other APs is much smaller than $1/W$. Based on Fisher information theory, the lower bound on the error covariance of $\boldsymbol{w} = [w_1, \dots w_{I-1}]^\top$ can now be shown to read

$$\boldsymbol{\Sigma}_{\text{diff}} = \frac{\lambda^2 N_0}{8\pi^2 E}(\mathbf{D} + \frac{\mathbf{1}\mathbf{1}^\top}{\rho_0^2}), \tag{4}$$

where $\mathbf{D}$ is a diagonal matrix whose m-th diagonal element is given by $[\mathbf{D}]_{m,m} = 1/\rho_m^2$, $\mathbf{1}$ is a vector of $I-1$ ones and the superscript $(.)^\top$ denotes the transpose operation.

As a baseline, we will devise and use the MLE. The vector of differential measurements in (3) can be expressed as

$$\boldsymbol{\delta} = \boldsymbol{h}(\boldsymbol{x}_{\text{ue}}) + \boldsymbol{w}, \tag{5}$$

where $\boldsymbol{\delta} = [\delta_1, \dots \delta_{I-1}]^\top$, $\boldsymbol{h}(\boldsymbol{x}_{\text{ue}}) = [h_1(\boldsymbol{x}_{\text{ue}}), \dots h_{I-1}(\boldsymbol{x}_{\text{ue}})]^\top$, $h_m(\boldsymbol{x}_{\text{ue}}) = \frac{-\lambda}{2\pi}(\text{mod}(-2\pi\|\boldsymbol{x}_{\text{ue}} - \boldsymbol{x}_{\text{ap},m}\|/\lambda, 2\pi) - \text{mod}(-2\pi\|\boldsymbol{x}_{\text{ue}} - \boldsymbol{x}_{\text{ap},0}\|/\lambda, 2\pi))$ and $\text{mod}(a, b)$ denotes the modulo operation of a with respect to b. Given that $\boldsymbol{w}$ follows a multivariate normal distribution with zero-mean and covariance matrix $\boldsymbol{\Sigma}_{\text{diff}}$, the likelihood function is $\mathcal{L}(\boldsymbol{\delta}|\boldsymbol{x}_{\text{ue}}) = \mathcal{N}(\boldsymbol{\delta}; h(\boldsymbol{x}_{\text{ue}}), \boldsymbol{\Sigma}_{\text{diff}})$. The MLE for the UE position can be obtained by minimizing the negative log-likelihood, given by

$$\widehat{\boldsymbol{x}}_{\text{ue}} = \underset{\boldsymbol{x}_{\text{ue}}}{\arg\min}\ (\boldsymbol{\delta} - \boldsymbol{h}(\boldsymbol{x}_{\text{ue}}))^\top \boldsymbol{\Sigma}_{\text{diff}}^{-1}(\boldsymbol{\delta} - \boldsymbol{h}(\boldsymbol{x}_{\text{ue}})). \tag{6}$$

The MLE has a notable computing complexity, quantified in Section IV, while serving as the performance benchmark.

III. Proposed NN-based Positioning Approaches

In this section, we introduce two NN-based positioning approaches, utilizing a total of three NNs. The first approach (referred to as direct phase-only CPP) employs a single MLP model that directly processes raw phase measurements to estimate the UE position. The second approach (referred to as integer ambiguity-aided CPP), consists of two NNs: an MLP-based model that estimates the integer ambiguities from phase measurements, and a CNN model that integrates these estimated ambiguities with phase measurements to determine the UE position.

A. Direct Phase-Only Carrier Phase Positioning

We first propose a straightforward approach to estimate the UE position using a *MLP-based positioning model*. The proposed MLP takes the differential measurements $\boldsymbol{\delta}$ in (5) as input and generates an estimate $\widehat{\boldsymbol{x}}_{\text{ue}}$ of the true UE position $\boldsymbol{x}_{\text{ue}}$. The loss function employed in this model is the mean-squared error (MSE), expressed as $\|\boldsymbol{x}_{\text{ue}} - \widehat{\boldsymbol{x}}_{\text{ue}}\|^2$. The proposed model is a fully connected NN composed of dense layers. The model consists of an input layer with a dimension of $I-1$ and the Rectified Linear Unit (ReLU) activation, followed by seven hidden layers with dimensions of A, $2A$, $4A$, $8A$, $4A$, $2A$, and A, all using the ReLU activation, and an output layer with a dimension of 2 and the linear activation function.

B. Integer Ambiguity-Aided Carrier Phase Positioning

The second approach first estimates the integer ambiguities using a MLP-based ambiguity estimation model.

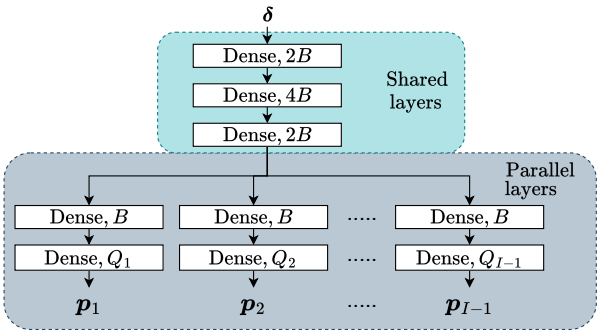

Fig. 2. Proposed MLP-based ambiguity estimation model: Rectangles represent dense layers with the number of neurons inside each rectangle and each branch generates a probability distribution.

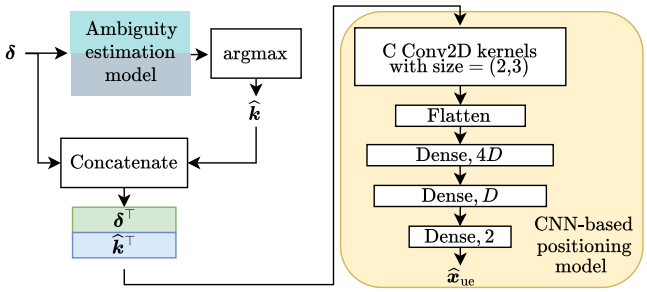

Fig. 3. Proposed CNN-based positioning model incorporating an MLP-based ambiguity estimation model and a variety of layer types.

The estimated ambiguities are then combined with phase measurements and fed into a CNN-based positioning model.

MLP-based ambiguity estimation model: We propose a MLP-based NN to generate a set of probability distributions $\boldsymbol{P} = [\boldsymbol{p}_1, \dots \boldsymbol{p}_{I-1}]^\top$ for the differential ambiguities $\boldsymbol{k} = [k_1, \dots, k_{I-1}]^\top$ from the differential measurements $\boldsymbol{\delta}$. Each differential ambiguity k_m is geometrically bounded by $[-q_m - 1, q_m] = [\lfloor -\|\boldsymbol{x}_{\text{ap},m} - \boldsymbol{x}_{\text{ap},0}\|/\lambda \rfloor, \lfloor \|\boldsymbol{x}_{\text{ap},m} - \boldsymbol{x}_{\text{ap},0}\|/\lambda \rfloor]$, where $\lfloor \cdot \rfloor$ denotes the floor function that returns the largest integer less than or equal to its argument. This results in $Q_m = 2q_m + 2$ possible labels for each differential ambiguity, with the total number of possible labels across all differential ambiguities given by $Q = \sum_{m=1}^{I-1} Q_m$. For each k_m, the model generates a probability distribution $\boldsymbol{p}_m = [p_{m,-q_m-1}, \dots p_{m,q_m}]^\top$, where $p_{m,l} \in [0, 1]$ represents the probability of the differential ambiguity k_m taking the integer value l, with $\sum_l p_{m,l} = 1$.

The proposed MLP structure is illustrated in Fig. 2. The input first propagates through shared layers, then the model is divided into parallel branches. The shared layers and the first layer of the parallel branches utilize the ReLU activation function, whereas the output layers of the parallel branches utilize softmax activation function to output the probability distributions. The sparse categorical cross-entropy is employed as the loss function, which can be expressed as

$$\mathcal{L}_{\text{SCCE}} = -\frac{1}{I-1} \sum_{m=1}^{I-1} \ln(p_{m,k_m}), \tag{7}$$

where p_{m,k_m} is the predicted probability of the correct integer label for each differential ambiguity and $\ln(.)$ is the natural logarithm.

CNN-based positioning model: We introduce a positioning model based on a CNN that estimates the UE position by integrating $\boldsymbol{\delta}$ with the estimated ambiguities $\widehat{\boldsymbol{k}} = [\widehat{k}_1, \dots, \widehat{k}_{I-1}]^\top$. These estimated ambiguities are obtained from the MLP-based ambiguity estimation model described in Section III-B, where the output probability distributions are processed through an argmax operation to yield the final integer estimates. Specifically, the argmax operation determines the predicted integer label for each differential ambiguity branch by selecting the class with the highest probability, i.e., $\widehat{k}_m = \arg\max_{l \in [-q_m - 1, q_m]} p_{m,l}$.

Fig. 3 illustrates the proposed CNN model structure. By noting that both $\boldsymbol{\delta}$ and $\widehat{\boldsymbol{k}}$ vectors have the shape of $(I-1, 1)$, the concatenated matrix $[\boldsymbol{\delta}, \widehat{\boldsymbol{k}}]^\top$ has the shape of $(2, I-1)$. The 2D-Convolutional (Conv2D) layer with the ReLU activation applies C different learnable filters with a shape of $(2, 3)$ to the input data, using zero padding and a stride of 1. The output of the Conv2D layer has the shape of $(1, I-3, C)$, which is then flattened to a vector of shape $(C(I-3), 1)$. Subsequently, dense layers with the ReLU activations are applied. Finally, the output layer with the linear activation produces the UE location estimate. Similar to the MLP-based positioning model, MSE serves as the loss function.

IV. Inference Complexity

In this section, the inference complexities of the MLE-based and NN-based approaches are evaluated. The metric used for this purpose is the FLOP count, which is a widely adopted metric [19]–[25]. In our analysis, each operation—whether an addition, a subtraction, or a multiplication—is counted as one FLOP following the approach in [24], [25].

Network pruning, the task of reducing the size of a network by selectively removing parameters, has gained significant attention to tackle the over-parameterization and redundancy in deep learning models [19], [26], [27]. In this work, layerwise magnitude-based pruning [28] is applied, where a portion of weight parameters with the lowest absolute values are pruned in each layer. This approach ensures that the sparsity level remains consistent across all layers. Moreover, if the FLOPs associated with bias additions and activation function in NN approaches are neglected, the pruning ratio can be directly applied to the number of FLOPs for each proposed NN. Note that, since the CNN-based positioning model incorporates the MLP-based ambiguity estimation model, the pruning ratios of both models should be explicitly considered when calculating the number of FLOPs in the CNN-based positioning model.

A. Maximum Likelihood Estimation Complexity

The task of finding $\widehat{\boldsymbol{x}}_{\text{ue}}$ that maximizes the MLE function can be accomplished via a 2D grid search over the simulation area. For simplicity, we neglect the complexity associated with calculating the term $\boldsymbol{h}(\boldsymbol{x}_{\text{ue}})$ in (6) and assume that $\boldsymbol{\Sigma}_{\text{diff}}^{-1}$ is

precomputed, focusing solely on the computational complexity of the term $(\boldsymbol{\delta} - \boldsymbol{h}(\boldsymbol{x}_{\text{ue}}))^{\top} \boldsymbol{\Sigma}_{\text{diff}}^{-1} (\boldsymbol{\delta} - \boldsymbol{h}(\boldsymbol{x}_{\text{ue}}))$. This operation entails $(I-1)$ subtractions, $I(I-1)$ multiplications, and $I(I-2)$ additions, resulting in a total computational cost of $2I^2 - 2I - 1$ FLOPs. When a 2D grid search is performed over N_{grid} points, the total computational cost for the MLE becomes

$$\mathcal{C}_{\text{MLE}} = N_{\text{grid}}(2I^2 - 2I - 1). \tag{8}$$

B. MLP-based Positioning Model Complexity

A dense layer with n_i input features and n_o neurons requires approximately $n_o(2n_i - 1) \approx 2n_o n_i$ FLOPs, with bias addition and activation costs being negligible for layers containing many neurons. As explained in Section III-A, the MLP-based positioning model is composed entirely of dense layers. Therefore, the number of FLOPs with a pruning rate of ρ_{MLP} is approximately $\mathcal{C}_{\text{MLP}} \approx \rho_{\text{MLP}} 168 A^2$.

C. MLP-based Ambiguity Estimation Model Complexity

Similar to the MLP-based positioning model, the MLP-based ambiguity estimation model described in Section III-B also consists of only dense layers. The total number of FLOPs with a pruning rate of ρ_{AE} can be calculated and expressed as

$$\mathcal{C}_{\text{AE}} \approx \rho_{\text{AE}} \left[32B^2 + (4B^2 + 4B) \times (I-1) + 2B \times Q \right]. \tag{9}$$

D. CNN-based Positioning Model Complexity

Applying an input data with shape $(2, I-1)$ to C filters each with shape $(2, 3)$ in the CNN-based positioning model in Section III-B costs $\mathcal{C}_{\text{CNN,c}} = 11C \times (I-3)$ FLOPs, where a dot product between a $(2, 3)$ filter and the corresponding input window costs 11 FLOPs. The number of FLOPs of the subsequent dense layers can be calculated as $\mathcal{C}_{\text{CNN,d}} \approx 8D^2 + 4D + 8CD(I-3)$. Also, since the CNN-based positioning model requires $\widehat{\boldsymbol{k}}$ to function as shown in Fig. 3, the complexity expression of the ambiguity estimation model in (9) should also be considered. With a pruning rate of ρ_{CNN} in the Conv2D layer and the subsequent dense layers, the total number of FLOPs is given by

$$\mathcal{C}_{\text{CNN}} = \rho_{\text{CNN}} \times (\mathcal{C}_{\text{CNN,c}} + \mathcal{C}_{\text{CNN,d}}) + \mathcal{C}_{\text{AE}}. \tag{10}$$

V. Numerical Results

We consider a square-shaped evaluation area of $100\,\text{m}^2$. A total of $I = 20$ antenna points are uniformly distributed at random over the area in order to stimulate a CF network architecture [12] as shown in Fig. 4. Similarly, one UE is placed uniformly at random in the area. The layer parameters of the NN models are set as $A = B = D = 128$ for dense layers and $C = 32$ for convolutional filters.

The other evaluation parameters include noise power spectral density (PSD) of –174 dBm/Hz, receiver noise figure of 13 dB, and uplink transmit powers of $\{-30, -20, -10, 0\}$ dBm. Also, the free space path-loss model is employed. The uplink pilot waveforms follow the 5G-NR sounding reference signal (SRS) specifications outlined in [29]. The center frequency is set to either

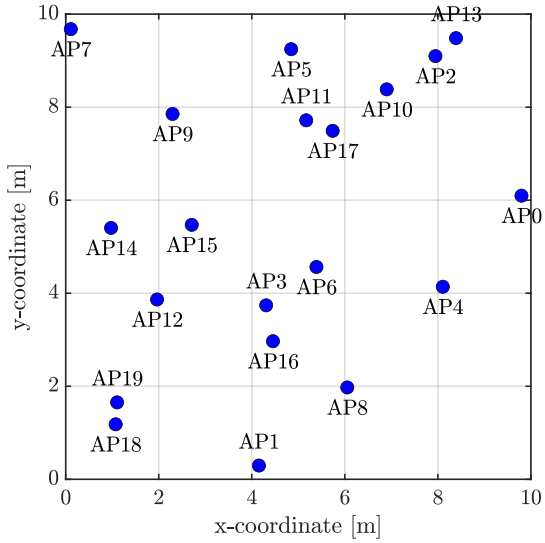

Fig. 4. Locations of the distributed APs in the evaluation region.

800 MHz or 1.8 GHz, with a subcarrier spacing of 15 kHz. The pilot transmission utilizes 4 resource blocks and a comb factor of 4, resulting in a utilized uplink reference signal bandwidth of 180 kHz. A single reference symbol configuration [29] is used, and the modulation scheme employed is BPSK. In our simulation scenario, the total number of possible labels across all differential ambiguities, Q, is calculated as 660 for a center frequency of 800 MHz and 1472 for 1.8 GHz.

A. Training of NN Models

The proposed NNs are trained separately for each transmit power and center frequency configuration, using 700×10^3 training samples and 150×10^3 validation samples per configuration. At each sample, a randomly drawn UE location is used. As a standard way of training procedure in supervised learning, true labels are used during the training phase of models, trained according to the input-output relationship of models explained in Section III.

The models are trained using a batch size of 1000 for 1000 epochs. The Adam optimizer is employed with a learning rate of 10^{-4}, and L2 regularization is applied with a coefficient of 10^{-5}. To decrease inference complexity, pruning is applied during training. The training process begins with an initial phase of 100 epochs without pruning. After this phase, between epochs 100 and 400, a polynomial decay pruning scheduler is employed, gradually pruning $\rho\%$ of the weight parameters, starting from an initial sparsity of zero and reaching a final sparsity of $\rho\%$ [30]. After pruning, the sparse network is retrained until epoch 1000, allowing the network to adjust and compensate for the removed weight parameters. Each model is first trained without pruning. Then, in subsequent training trials, the pruning rate is increased by steps of 25%, with the pruning rate being increased to the point where model performance remains largely unaffected.

TABLE I
PRUNING RATES AND INFERENCE FLOP NUMBERS

Direct Phase-Only Carrier Phase Positioning			
NN Model	Frequency	Pruning Rate	FLOP number
MLP-based positioning	800 MHz	50%	1.376×10^6
MLP-based positioning	1.8 GHz	50%	1.376×10^6
Integer Ambiguity-Aided Carrier Phase Positioning Approach			
NN Model	Frequency	Pruning Rate	FLOP number
MLP-based ambiguity estimation	800 MHz	50%	0.974×10^6
CNN-based positioning	800 MHz	75%	1.148×10^6
MLP-based ambiguity estimation	1.8 GHz	0%	2.156×10^6
CNN-based positioning	1.8 GHz	75%	2.330×10^6

The optimal pruning rate varies based on the complexity of the problem for each frequency and NN model.

Table I presents the pruning rates and the corresponding FLOP counts for the two proposed approaches, along with the NN models included at the two frequencies. As discussed in Section IV-D, for a given frequency, the FLOP count of the CNN-based positioning model includes the FLOP count of the MLP-based ambiguity estimation model at the same frequency.

B. Parametrization of MLE Benchmarks

As a first approach, to ensure a fair comparison with the proposed NN approaches, the number of grid points (N_{grid} in (8)) should be chosen to match the FLOP number shown in Table I. After finding the required N_{grid} values, they are rounded up to ensure that N_{grid} is a perfect square, allowing the grid points to be distributed uniformly in a square area with equal spacing in both dimensions.

As an alternative approach, we calculate the complexity reduction factor of the proposed NNs by determining the required N_{grid} values needed to achieve comparable positioning performance. In both MLE approaches, after identifying the grid point that maximizes the MLE, a gradient descent algorithm with 100 steps is used to fine-tune the estimation.

C. Ambiguity Estimation Results

To evaluate the performance of the MLP-based ambiguity estimation model, we define two accuracy metrics, namely element-wise accuracy and overall accuracy, over T test samples. The element-wise accuracy is given by

$$\text{Acc}_e = \frac{1}{T}\frac{1}{I-1}\sum_{t=1}^{T}\sum_{m=1}^{I-1}\mathbb{I}(\widehat{k}_{m,t} = k_{m,t}) \times 100\%, \quad (11)$$

where $\widehat{k}_{m,t}$ and $k_{m,t}$ are the estimated and true ambiguities $\widehat{k}_m$ and k_m for the test sample t, respectively, and $\mathbb{I}(\cdot)$ is the indicator function, which equals 1 when its argument is true and 0 otherwise. The overall accuracy is, in turn, defined as

$$\text{Acc}_o = \frac{1}{T}\sum_{t=1}^{T}\mathbb{I}(\widehat{\boldsymbol{k}}_t = \boldsymbol{k}_t) \times 100\%, \quad (12)$$

TABLE II
ACCURACY PERFORMANCE OF AMBIGUITY ESTIMATOR MODELS

		Transmit Power [dBm]			
Metric	**Frequency**	–30	–20	–10	0
Acc_e	800 MHz	98.97%	99.57%	99.83%	99.89%
	1.8 GHz	92.64%	97.90%	99.08%	99.43%
Acc_o	800 MHz	83.72%	92.97%	97.24%	98.40%
	1.8 GHz	32.74%	71.13%	86.48%	91.59%

where $\widehat{\boldsymbol{k}}_t$ and $\boldsymbol{k}_t$ are the estimated and true ambiguity vectors for the test sample t, respectively.

The accuracy results, evaluated over $T = 150 \times 10^3$ test samples for the considered frequencies and UE transmit power levels, are presented in Table II. The accuracy decreases at the higher frequency of 1.8 GHz compared to 800 MHz, which can be attributed to the increased number of integer ambiguities that must be resolved. However, overall, the obtained accuracies are high, reflecting accurate ambiguity resolution.

D. Positioning Results

Root mean-squared error (RMSE)-based positioning results are calculated based on 150×10^3 test samples. A comparison of the proposed MLP-based and CNN-based positioning models with the corresponding MLE counterparts, is presented in Fig. 5 for frequencies of 800 MHz and 1.8 GHz. The impact of ambiguity estimation on CNN-based positioning model performance was evaluated by comparing scenarios utilizing true ambiguities versus estimated ambiguities. Both CNN- and MLP-based models demonstrate superior performance compared to their respective MLE counterparts, each matched in inference complexity. This superiority can be attributed to MLE's limitations under constrained grid search parameters designed to maintain comparable inference complexity across NN models.

As illustrated in Fig. 5, the CNN-based model outperforms the MLP-based model despite reduced inference complexity as seen in Table I at 800 MHz. Notably, the CNN-based model employing estimated ambiguities achieves a RMSE of 1 cm at 0 dBm transmit power. Fig. 5 reveals that while the CNN-based model exhibits lower performance than the MLP-based model at low transmit power, it outperforms the MLP-based model when transmit power exceeds –20 dBm at 1.8 GHz. However, at 1.8 GHz, the CNN-based model requires greater inference complexity compared to the MLP-based model (cf. Table I). Additionally, the performance difference between CNN models utilizing estimated versus true ambiguities is more pronounced at 1.8 GHz, primarily due to the somewhat reduced accuracy of the ambiguity estimation model at this frequency (cf. Table II).

The required N_{grid} values for the MLE to achieve similar performance as the proposed NNs are found to be $750^2 = 0.5625 \times 10^6$ and $1800^2 = 3.24 \times 10^6$ for 800 MHz and 1.8 GHz, respectively. For MLP-based positioning, the inference complexity reduction factors are approximately

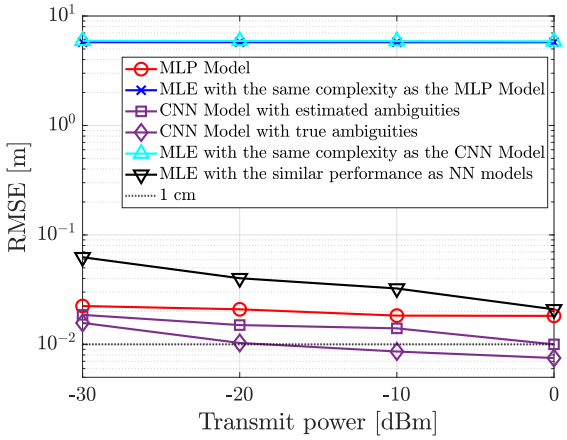

(a) 800 MHz distributed deployment

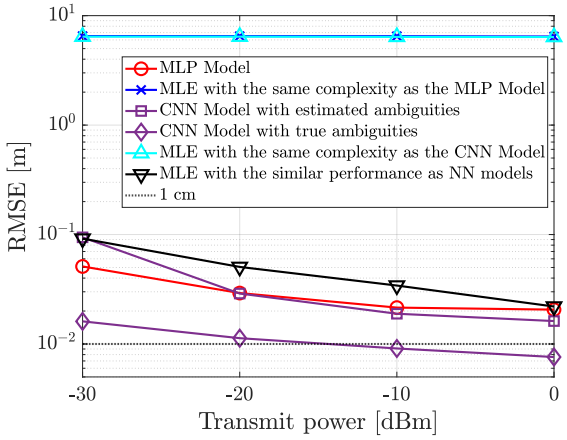

(b) 1.8 GHz distributed deployment

Fig. 5. Positioning accuracy results and comparison between the two proposed NNs and their MLE counterparts.

310 at 800 MHz and 1787 at 1.8 GHz, while for CNN-based positioning, the factors are around 372 and 1055 at 800 MHz and 1.8 GHz, respectively. Due to the need for a very dense grid search at higher frequencies with MLE, the complexity reduction factors through the proposed methods are significantly higher at 1.8 GHz – being already three orders of magnitude. Furthermore, the optimal NN that maximizes the reduction factor varies depending on the frequency.

To conduct a more comprehensive analysis, the positioning error empirical cumulative distribution function (ECDF) curves of the proposed NNs at a transmit power of 0 dBm are illustrated in Fig. 6. In the MLP model, increasing the frequency notably degrades the positioning performance. In contrast, the CNN model demonstrates improved performance at higher frequencies, with more ECDF values below approximately 1.4 cm. Beyond this threshold, the lower frequency exhibits superior performance, which can be attributed to the ambiguity estimation accuracy at these frequencies. The 95th percentile positioning errors for the CNN model are 2.08 cm at 800 MHz and 3.08 cm at 1.8 GHz, whereas the MLP model exhibits errors of 4.01 cm at 800 MHz and 4.34 cm at 1.8 GHz.

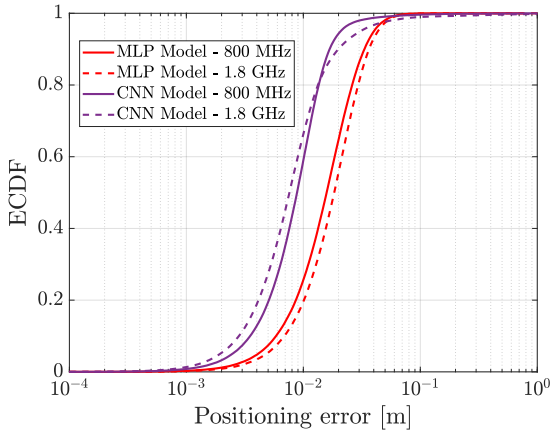

Fig. 6. ECDF of the proposed NNs at a transmit power of 0 dBm.

VI. Conclusion

This paper introduced and proposed two deep learning-based approaches for uplink carrier phase positioning that rely exclusively on distributed uplink phase observations in a cell-free system – allowing to avoid classical ToA measurements and the related challenges with clock biases. Our results show that both proposed approaches outperform traditional MLE benchmark method under the constraint of comparable inference complexity. Specifically, the CNN-based model achieves superior accuracy at higher transmit power levels and demonstrates a positioning error of approximately 1 cm at 0 dBm UE transmit power at 800 MHz. However, its performance is also more sensitive to ambiguity estimation accuracy at higher frequencies (1.8 GHz). In contrast, the MLP-based model exhibits more stable performance than the CNN-based model across varying power levels. These findings highlight the potential of deep learning for efficient and precise phase-only positioning in future cell-free systems, paving the way for improved localization in environments where ToA-based methods are impractical. Our future work will focus on studying and mitigating the impacts of multipath and residual phase-calibration errors at the network side.

VII. Acknowledgement

This work was supported by the MiFuture project under the HORIZON-MSCA-2022-DN-01 call (Grant number: 101119643), and by the SNS JU project 6G-DISAC under the EU's Horizon Europe research and innovation Program under Grant Agreement No 101139130. The work was also in part supported by Business Finland under the 6G-ISAC project, and in part by the Research Council of Finland under the grant 359095.

References

[1] N. González-Prelcic *et al.*, "The integrated sensing and communication revolution for 6G: Vision, techniques, and applications," *IEEE Proc.*, vol. 112, no. 7, pp. 676–723, 2024.

[2] W. Ding, W. Sun, Y. Gao, and J. Wu, "Carrier phase-based precise heading and pitch estimation using a low-cost GNSS receiver," *Remote Sensing*, vol. 13, no. 18, p. 3642, 2021.

[3] H.-S. Cha *et al.*, "5G NR positioning enhancements in 3GPP release-18," *IEEE Commun. Stand. Mag.*, vol. 9, no. 1, pp. 22–27, 2025.

[4] 3GPP, "Study on Expanded and Improved NR Positioning (Release 18)," Tech. Rep. TR 38.859, June 2024.

[5] J. Nikonowicz, A. Mahmood, M. I. Ashraf, E. Björnson, and M. Gidlund, "Indoor positioning in 5G-Advanced: Challenges and solution toward centimeter-level accuracy with carrier phase enhancements," *IEEE Wireless Commun.*, vol. 31, no. 4, 2024.

[6] S. Fan, W. Ni, H. Tian, Z. Huang, and R. Zeng, "Carrier phase-based synchronization and high-accuracy positioning in 5G new radio cellular networks," *IEEE Trans. Commun.*, vol. 70, no. 1, pp. 564–577, 2022.

[7] J. Talvitie, M. Säily, and M. Valkama, "Orientation and location tracking of XR devices: 5G carrier phase-based methods," *IEEE J. Sel. Topics Signal Process.*, vol. 17, no. 5, pp. 919–934, 2023.

[8] K. Berntorp, A. Weiss, and S. D. Cairano, "Integer ambiguity resolution by mixture Kalman filter for improved GNSS precision," *IEEE Trans. Aerosp. Electron. Syst.*, vol. 56, no. 4, pp. 3170–3181, 2020.

[9] A. Hassibi and S. Boyd, "Integer parameter estimation in linear models with applications to GPS," *IEEE Trans. Signal Process.*, vol. 46, no. 11, pp. 2938–2952, 1998.

[10] R. de Celis, P. Solano-Lopez, J. Barroso, and L. Cadarso, "Neural network-based ambiguity resolution for precise attitude estimation with GNSS sensors," *IEEE Trans. Aerosp. Electron. Syst.*, vol. 60, no. 5, pp. 6702–6716, 2024.

[11] Z. Zhang, X. Li, and H. Yuan, "Best integer equivariant estimation based on unsupervised machine learning for GNSS precise positioning and navigation in complex environments," *IEEE Trans. Aerosp. Electron. Syst.*, vol. 60, no. 3, pp. 2672–2682, 2024.

[12] Ö. T. Demir, E. Björnson, and L. Sanguinetti, "Foundations of user-centric cell-free massive MIMO," *Foundations and Trends® in Signal Processing*, vol. 14, no. 3-4, pp. 162–472, 2021.

[13] Z. Wang *et al.*, "A tutorial on extremely large-scale MIMO for 6G: Fundamentals, signal processing, and applications," *IEEE Commun. Surveys Tuts.*, vol. 26, no. 3, pp. 1560–1605, 2024.

[14] A. Fascista *et al.*, "Joint localization, synchronization and mapping via phase-coherent distributed arrays," *IEEE J. Sel. Topics Signal Process.*, pp. 1–16, *(early access)* 2025.

[15] N. Vukmirovic, M. Eric, M. Janjic, and P. M. Djuric, "Direct wideband coherent localization by distributed antenna arrays," *Sensors*, vol. 19, no. 20, 2019.

[16] H. Wymeersch, R. Amiri, and G. Seco-Granados, "Fundamental performance bounds for carrier phase positioning in cellular networks," in *Proc. IEEE GLOBECOM*, Kuala Lumpur, Malaysia, 2023, pp. 7478–7483.

[17] B. Deutschmann *et al.*, "Accurate direct positioning in distributed mimo using delay-doppler channel measurements," in *Proc. IEEE SPAWC*, Lucca, Italy, 2024, pp. 606–610.

[18] A. Guerra, F. Guidi, D. Dardari, and P. M. Djurić, "Near-field tracking with large antenna arrays: Fundamental limits and practical algorithms," *IEEE Trans. Signal Process.*, vol. 69, pp. 5723–5738, 2021.

[19] D. Blalock, J. J. Gonzalez Ortiz, J. Frankle, and J. Guttag, "What is the state of neural network pruning?" *Proc. of Machine Learning and Syst.*, vol. 2, pp. 129–146, 2020.

[20] K. He, X. Zhang, S. Ren, and J. Sun, "Deep residual learning for image recognition," in *Proc. IEEE CVPR*, June Las Vegas, NV, USA, 2016.

[21] P. Molchanov, A. Mallya, S. Tyree, I. Frosio, and J. Kautz, "Importance Estimation for Neural Network Pruning," in *Proc. IEEE/CVF CVPR*, Los Alamitos, CA, USA, Jun. 2019, pp. 11 256–11 264.

[22] Y. Wu, U. Gustavsson, M. Valkama, A. G. i. Amat, and H. Wymeersch, "Time vs. frequency domain DPD for massive MIMO: Methods and performance analysis," *IEEE Trans. Wireless Commun.*, pp. 1–1, 2025.

[23] P. Cong and C. Yang, "Number of FLOPs of training DNNs for learning precoding," in *Proc. IEEE VTC-Spring*, Florence, Italy, 2023, pp. 1–6.

[24] A. S. Tehrani *et al.*, "A comparative analysis of the complexity/accuracy tradeoff in power amplifier behavioral models," *IEEE Trans. Microwave Theory Techn.*, vol. 58, no. 6, pp. 1510–1520, 2010.

[25] L. Salaün and H. Yang, "Deep learning based power control for cell-free massive MIMO with MRT," in *Proc. IEEE GLOBECOM*, Madrid, Spain, 2021.

[26] M. Denil, B. Shakibi, L. Dinh, M. Ranzato, and N. De Freitas, "Predicting parameters in deep learning," *Advances in Neural Information Processing Systems*, vol. 26, 2013.

[27] Z. Liu, M. Sun, T. Zhou, G. Huang, and T. Darrell, "Rethinking the value of network pruning," in *International Conference on Learning Representations*, 2019. [Online]. Available: https://openreview.net/forum?id=rJlnB3C5Ym

[28] S. Han, J. Pool, J. Tran, and W. Dally, "Learning both weights and connections for efficient neural network," *Advances in Neural Information Processing Systems*, vol. 28, 2015.

[29] 3GPP, "Physical Channels and Modulation (Release 18)," Tech. Spec. TS 38.211, v18.5.0, Dec. 2024.

[30] M. Zhu and S. Gupta, "To prune, or not to prune: exploring the efficacy of pruning for model compression," 2017. [Online]. Available: https://arxiv.org/abs/1710.01878